

Chapter 27

Interaction Between Aerothermally Compliant Structures and Boundary Layer Transition

Zachary B. Riley and Jack J. McNamara

Abstract The inherent relationship between boundary layer stability, aerodynamic heating, and surface conditions make the potential for interaction between the structural response and boundary layer transition an important and challenging area of study in high speed flows. This interdependence implies that accurate structural response prediction of a hypersonic vehicle necessitates an aerothermoelastic analysis that accounts for boundary layer stability in regions where transition is likely to occur. This study focuses on this problem by incorporating a time-varying boundary layer state into the aerothermoelastic response prediction of a structural panel in hypersonic flow. Results demonstrate that rearward movement of the boundary layer transition front reduces thermal loading to the panel and peak deformation, potentially extending the life of the structure.

Keywords Fluid-thermal-structural-interactions • Boundary layer transition • Hypersonic • Aerothermoelastic • Hot structure

27.1 Introduction

Load bearing thermal protection systems, in the form of thin-gauge metallic airframes, provide a means to minimize the weight and improve the serviceability of reusable, long duration cruise hypersonic aircraft [1–5]. However, the compliant nature of these structures, in combination with the severe aerothermodynamic loading, results in a propensity for nonlinear fluid-structural interactions. Due to this interaction, the boundary layer state (laminar, transitional, or turbulent) is dependent on the structural response. Accurate determination of the aerodynamic heat load, which varies significantly with the state of the boundary layer, is detrimental to structural life prediction and optimal weight design [2–5]. Therefore, the future design of hypersonic aircraft may necessitate aerothermoelastic analysis which accounts for the state of the boundary layer.

Boundary layer stability is highly dependent on wall temperature [6, 7] and surface geometry [7–17], both of which vary during flight for hot structure hypersonic vehicles. Previous studies have examined how aerothermoelastic effects, such as thermally induced deformations, can augment aerothermal loads [18, 19] and impact boundary layer transition [20, 21]. Through wind-tunnel testing of X-33 configurations, Berry et al. [20] concluded that a three-dimensional array of bowed panels was less effective at forcing transition onset than discrete roughness. In a recent study, Riley et al. [21] numerically assessed the boundary layer stability of flow past large-scale, two-dimensionally (2-D) varying surface topologies resembling deformations of surface panels using the linear Parabolized Stability Equations. This study indicated that series of panels, deformed into the flow, significantly disrupts the unstable growth of disturbances excited in the absence of the deformations. The potential for 2-D wavy walls to stabilize hypersonic boundary layers has also been observed for roughness scale deformations [12–17]. As the vehicle response alters the boundary layer state, this in turn affects the aerothermal loads acting on the structure.

A few studies have examined how transitional fluid loading impacts structural response. Lamorte and Friedmann [22] assessed how transition location, and its associated uncertainty, impacts the aerothermoelastic stability of a wing structure subject to transitional aerodynamic heating. Additionally, Riley et al. [23] examined how transition onset location, transition length, and transitional heat flux and fluctuating pressure that exceed (or *overshoot*) turbulent values affect the structural response of surface panels. These studies found that transitional flows can result in aerothermal loads and structural responses which exceed that predicted assuming turbulent loading conditions.

These previous studies indicate that boundary layer stability is sensitive to changes in surface conditions and that the structural response is strongly dependent on the boundary layer state (laminar, transitional, turbulent). This interdependence

Z.B. Riley • J.J. McNamara (✉)
The Ohio State University, Columbus, OH 43210-1276, USA
e-mail: mcnamara.190@osu.edu

implies that accurate structural response prediction of a hypersonic vehicle necessitates an aerothermoelastic analysis that incorporates boundary layer stability analysis in transitional flow regions. Thus, this paper focuses on examination of the coupled problem by carrying out an aerothermoelastic analysis of a panel for the case of a time-varying boundary layer transition location. Completion of this study provides improved insight into the degree of aerothermoelastic coupling required in the design and analysis of hypersonic vehicles.

27.2 Methodology

An overview of the aerothermoelastic framework used to obtain the panel response is provided in Sect. 27.2.1. The transitional aerothermodynamic load models are discussed in Sect. 27.2.2. Finally, the specific problem examined in this paper is described in Sect. 27.2.3.

27.2.1 Aerothermoelastic Model

The aerothermoelastic model, depicted in Fig. 27.1, has three primary components: (1) aerothermodynamic loads, (2) structural dynamics, and (3) heat transfer. The aerothermodynamics drive the thermo-structural response through the application of a pressure load (composed as the summation of mean and fluctuating components) and a surface heat flux. The mean flow pressure is modeled using third-order piston theory [24–26] which accounts for changes in the mean pressure due to structural deformations. The fluctuating pressure load (FPL) is computed using the model discussed in Sect. 27.2.2.3. This framework was previously used to assess the impact of transitional heat flux and fluctuating pressure loads on panel response, where the transition onset and length were prescribed prior to the simulation [23]. The heat flux is modeled using Eckert’s reference enthalpy method [27]. Note that the FPL and heat flux are dependent on the boundary layer edge properties, which are obtained from the mean flow pressure in conjunction with isentropic flow relations [24]. The aerothermoelastic model is currently being modified, as shown by the dashed lines in Fig. 27.1, to incorporate a transition prediction surrogate such that the transition onset location may vary in time; either with a prescribed variation or as a function of the structural response. For this study, only the prescribed variation in time is considered.

The structure is modeled as cylindrical bending of an isotropic plate with the assumptions of von Kármán moderate deflection plate theory [24]. The formulation includes the effects of thermal loading due to non-uniform (in-plane and through-thickness) temperature distributions, chord-wise variation of the modulus of elasticity and thermal expansion coefficient, rotary inertia, and Rayleigh damping. The structural equation of motion is discretized using Galerkin’s method. The transverse displacement is approximated as a series of free-vibration mode shapes of the panel that satisfy pinned boundary conditions. Note that due to the kinematic constraints, the in-plane thermal effects are primarily driven by the chord-wise average temperature [28].

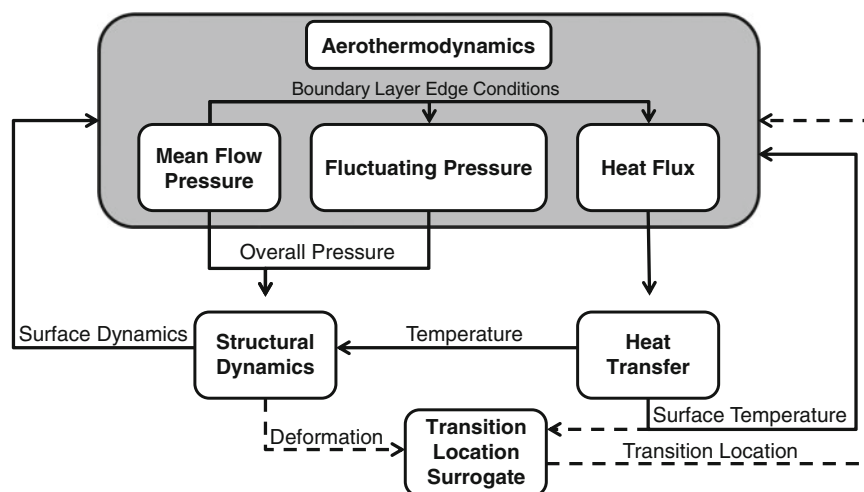


Fig. 27.1 Enhanced aerothermoelastic model

As shown in Fig. 27.1, the structural temperature is computed from a heat transfer analysis. This is carried out by solving a finite element formulation of the transient, 2-D heat transfer equation with temperature-dependent specific heat and thermal conductivity [28]. The 2-D formulation allows for heat conduction through both the thickness and length of the panel. An adiabatic wall condition is prescribed for each boundary of the panel, except the upper surface where the aerodynamic heat flux is applied.

The aerothermal and aeroelastic solvers are linked using a loosely coupled partitioned approach. This scheme is advantageous in terms of computational efficiency as the individual solvers can use different time steps and information is exchanged between the solvers only once per time step [29]. In-depth descriptions of the aerothermoelastic model formulation are provided in [24, 28]. Further information regarding the coupling procedure and numerical schemes implemented in the aerothermoelastic model is given in [29, 30].

27.2.2 Transitional Aerothermodynamic Loads

In this study, the aerothermodynamic loads acting on the panel are heat flux and an overall pressure load (comprised of a mean and fluctuating component). Transitional boundary layer effects are incorporated into the heat flux and fluctuating pressure through blending laminar and turbulent profiles in proportion to an intermittency function, which represents the fraction of time any spatial location spends in turbulent flow [31]. A brief description of the intermittency function is given in Sect. 27.2.2.1. Details on the transitional heat flux and fluctuating pressure models are provided in Sects. 27.2.2.2 and 27.2.2.3.

27.2.2.1 Intermittency

Transition from laminar to turbulent flow is, in general, not an abrupt process. It occurs over a finite length due to the growth, propagation, and interaction of turbulent spots [32]. As a result, the flow during transition can be characterized as a laminar boundary layer subject to intermittent patches of turbulence. Thus, the statistical flow properties in the transition region can be described using an intermittency function which represents the fraction of time any spatial location spends in turbulent flow. The intermittency throughout the transition region is computed using Eq. (27.1), which is derived from Emmon's probabilistic model [32, 33] with the assumption that the burst source-rate density can be described as a Dirac delta function. This form of the source-rate density function assumes the hypothesis of concentrated breakdown is valid [34], implying that turbulent spots are formed only at the transition onset location x_t . However, at the transition onset location turbulent spots may form randomly in time and in the spanwise direction. The intermittency distribution in Eq. (27.1) is a function of the edge velocity U_e (assumed constant over the transition region), the transition onset location x_t , the number of turbulent spots per unit time and spanwise distance n , and a spot propagation parameter σ . The spot propagation parameter is defined in Eq. (27.2), where $u_g = u_l - u_t$, $u_c = 1/2(u_l + u_t)$, u_l and u_t are the leading and trailing edge velocities of the turbulent spot, and α is the half angle.

$$\gamma(x) = 1 - \exp\left[-\frac{\sigma n}{U_e}(x - x_t)^2\right] \quad (27.1)$$

$$\sigma = \frac{u_g U_e}{u_c u_t} \tan \alpha \quad (27.2)$$

From the definition of intermittency, the length of the transition region Δx_t can be expressed as shown in Eq. (27.3). Introducing Δx_t into the exponent in Eq. (27.1), results in an expression for the intermittency which is a function of the transition onset and length alone.

$$\Delta x_t = (x - x_t)|_{\gamma=0.99} - (x - x_t)|_{\gamma=0.01} = 2.0457 \sqrt{\frac{U_e}{\sigma n}} \quad (27.3)$$

$$\gamma(x) = 1 - \exp\left[-\frac{4.1850}{\Delta x_t^2}(x - x_t)^2\right] \quad (27.4)$$

27.2.2.2 Heat Flux

The transitional heat flux is approximated by using the intermittency to blend the laminar and turbulent values as shown in Eq. (27.5). If the laminar and turbulent boundary layers originate at the same location, the blending in Eq. (27.5) can not account for transitional overshoot in heat flux [34]. Overshoot can be incorporated by assuming the turbulent boundary layer begins at a virtual origin $turb_{VO}$ corresponding to the transition onset location [31]. Applying the linear blending in Eq. (27.5) and assuming the turbulent boundary layer originates at x_t , Dhawan and Narasimha [31] matched experimental skin friction coefficients and displacement thickness during transition.

$$Q_{tran} = (1 - \gamma)Q_{lam} + \gamma Q_{turbvo} \quad (27.5)$$

Previous experiments, which have observed transitional overshoot in heat flux [35], demonstrate that heating rates decrease back to fully turbulent conditions beyond the overshoot region. To model this, the transitional heat flux [computed using Eq. (27.5)] is blended with the fully turbulent heating rates as shown in Eq. (27.6), where Λ is a Gaussian function, defined in Eq. (27.7). The peak of the Gaussian function coincides with the end of transition x_{te} , and the Full Width at Half Maximum β is specified such that the function decreases to negligible values prior to the end of the geometry x_{end} . This ensures that fully turbulent heating rates are obtained on the end of the geometry.

$$Q(x) = (1 - \Lambda)Q_{turb} + \Lambda Q_{tran} \quad (x_{te} \leq x \leq x_{end}) \quad (27.6)$$

$$\Lambda(x) = \exp\left[\frac{-\left(\frac{x-x_{te}}{x_{end}-x_{te}}\right)^2}{2\beta^2}\right] \quad (27.7)$$

$$\beta = \frac{0.5}{2\sqrt{2\ln 2}} \quad (27.8)$$

An example of the transitional heat flux generated using this model is provided in Fig. 27.2 for transition beginning at $x/L = 0.3$ and ending at $x/L = 0.5$. The “No overshoot” line in Fig. 27.2 corresponds to the transitional heat flux profile obtained using Eq. (27.5) if the laminar and turbulent boundary layers have the same origin. The “Overshoot” heat flux was generated assuming the turbulent boundary layer originates at $x/L = 0.3$ with the Gaussian blending applied in the turbulent region ($x/L \geq 0.5$). The heat flux profiles in Fig. 27.2 demonstrate that, through shifting the turbulent boundary layer origin, this model can be used to generate heat flux profiles which either account for or neglect the effect of transitional overshoot.

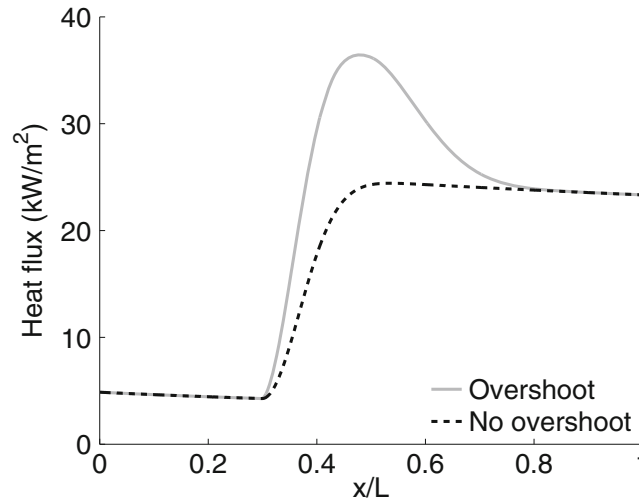


Fig. 27.2 Transitional heat flux model $x_t = 0.30$ m and $\Delta x_t = 0.20$ m

27.2.2.3 Fluctuating Pressure

The fluctuating pressure load model currently implemented in the aerothermoelastic solver is a modified version of the semi-empirical model developed by Deshmukh et al. [36]. The unsteady pressure is expressed as shown in Eq. (27.9), where $f(x, t)$ and $\Theta(x, t)$ represent the magnitude and phase angle of the pressure load.

$$p = f(x, t)e^{i\Theta(x, t)} \quad (27.9)$$

As denoted in Eq. (27.10), the phase angle is decomposed into separate temporal τ and spatial ψ components where the spatial variation is assumed relative to the leading edge of the panel. The temporal phase angles account for the phase lag between disturbances of different frequency at the same spatial location. Conversely, the spatial phase angles account for the phase lag between disturbances of the same frequency at different spatial locations. In this study, the phase angles (τ and ψ) are assumed to vary randomly with x and t , respectively. Recent work indicates that the impact of the boundary layer induced pressure fluctuation on structural response is dependent on the spatial phase angle model [36]. Therefore, the assumption of a random spatial phase angle, which neglects coherence in the boundary layer, introduces uncertainty into the predicted structural responses. The amplitude $f(x, t)$ is described as the combination of a root mean square (RMS) value, corresponding to the magnitude, and a power spectral density (PSD), corresponding to the frequency content [37–39].

$$\Theta(x, t) = \tau(t) + \psi(x) \quad (27.10)$$

The transitional boundary layer RMS pressure \tilde{p} is modeled using Eq. (27.11), which is a modified version of Laganelli's relation for turbulent boundary layer attached flow [37–39]. As shown in Eq. (27.11), the RMS pressure is a function of the dynamic pressure at the boundary layer edge q_e , a compressible flow transformation function F_c , a viscosity/velocity power law exponent λ , and a compressibility exponent b . Laganelli's relation was modified to increase the incompressible fluctuating pressure intensity from 0.006 to 0.009, as recommended by Bull [40] and Beresh et al. [41]. The second modification introduces an $Re_\theta^{-0.1}$ dependence into the RMS pressure calculation, which Beresh et al. [41] found to exist for Mach numbers between 2 to 3. Note that, $Re_\theta|_{\bar{x}^*}$ represents a normalization constant that specifies the spatial location at which the Re_θ dependence begins. The final modification incorporates a dependence on the local skin friction coefficients corresponding to transitional $c_{f_{tran}}$ and fully turbulent $c_{f_{turb}}$ boundary layers. The relationship in Eq. (27.11) is similar to Laganelli's model for turbulent boundary layer pressure fluctuations on rough surfaces [38], which scales the smooth wall RMS pressure based off the skin friction ratio to obtain the rough wall RMS pressure. As shown in Eq. (27.12), the transitional skin friction coefficient is computed in the same manner as the heat flux. To remove leading edge effects, the RMS pressure in the laminar region is specified as the minimum RMS value prior to transition onset.

$$\frac{\tilde{p}}{q_e} = 0.009 F_c^{\lambda(1+b)} \left(\frac{Re_\theta}{Re_\theta|_{\bar{x}^*}} \right)^{-0.1} \frac{c_{f_{tran}}}{c_{f_{turb}}} \quad (27.11)$$

$$c_{f_{tran}} = (1 - \gamma)c_{f_{lam}} + \gamma c_{f_{turbVO}} \quad (27.12)$$

The PSD ϕ is computed using Eq. (27.13), where δ_1 represents the boundary layer displacement thickness and ω corresponds to angular frequency. The fluctuating pressure load, acting on the panel, is obtained by converting the frequency domain PSD values and phase angles to a time domain signal using the analytical function provided in Eq. (27.14). This function is the real component of a one-sided Inverse Fourier Transform, where the upper limit of integration ω_{max} corresponds to the largest frequency expected to impact the structure. As energy is removed due to the frequency truncation, the pressure signal must be computed using a scaled PSD [Eq. (27.15)] in order to reproduce a fluctuating pressure which matches the input RMS values.

$$\frac{\phi(x, \omega) U_e}{q_e^2 \delta_1} = \frac{(\tilde{p}/q_e)^2 F_c^{-2\lambda} (2/\pi)}{1 + (F_c^{-2\lambda} \omega \delta_1 / U_e)^2} \quad (27.13)$$

$$p(x, t) = \int_0^{\omega_{max}} \sqrt{2\phi^*(x, \omega) \Delta\omega} \cos(\omega t + \Theta(x, \omega)) d\omega \quad (27.14)$$

$$\phi^*(x, \omega) = \frac{\tilde{p}^2}{\int_0^{\omega_{max}} \phi(x, \omega) d\omega} \phi(x, \omega) \quad (27.15)$$

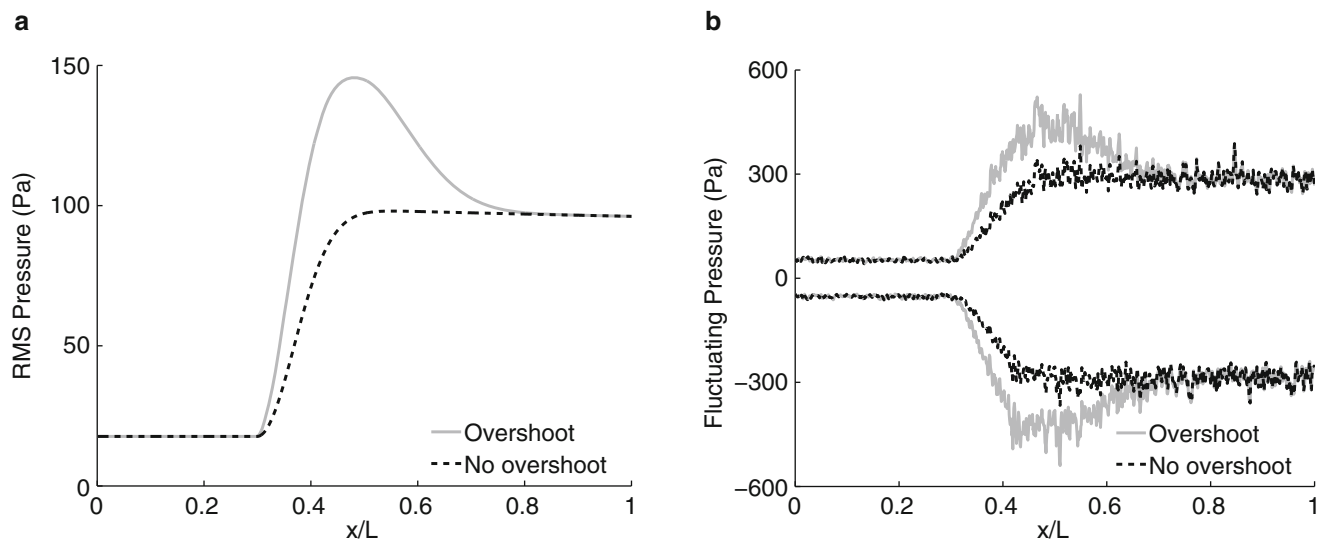


Fig. 27.3 Transitional fluctuating pressure load model. (a) RMS of fluctuating pressure. (b) Fluctuating pressure snapshot envelope

Table 27.1 Freestream conditions and panel geometry

Mach number	4.0
Altitude	30 km
Unit Reynolds number	$1.461\text{e}6 \text{ m}^{-1}$
Turn angle	5.0°
Length	1.00 m
Thickness	2.50 mm
Material	Aluminum 7075

An example of the transitional pressure load is provided in Fig. 27.3 in terms of the RMS pressure (Fig. 27.3a) and a snapshot of the fluctuating pressure envelope (Fig. 27.3b), for transition beginning at $x/L = 0.3$ and ending at $x/L = 0.5$. As with the heat flux profiles in Fig. 27.2, results are presented for shifted and unshifted turbulent boundary layers to demonstrate the effect of accounting for or neglecting transitional overshoot. The RMS pressure in Fig. 27.3a demonstrates that the present formulation results in a smooth spatial variation in the RMS pressure throughout transition, with peak magnitudes occurring at the end of transition. The fluctuating pressure envelope in Fig. 27.3b represents the minimum and maximum bounds of the instantaneous pressure load acting on the panel.

27.2.3 Problem Description

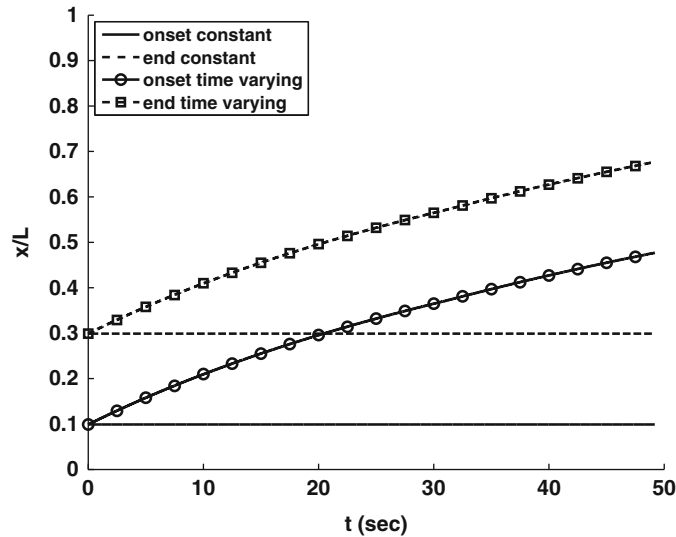
The freestream conditions and panel geometry considered in this study are listed in Table 27.1. It is assumed that the panel lies 1 m downstream of the leading edge of a wedge with a 5.0° half angle. Therefore, the flow the panel experiences corresponds to the post oblique shock conditions (i.e. $M = 3.64$). The material properties of the panel are listed in Table 27.2. Note that the modulus of elasticity, specific heat capacity, thermal conductivity, and thermal expansion coefficient are temperature-dependent properties where the listed values correspond to a temperature of 300 K. The numerical parameters used in this study, listed in Table 27.3, were determined through a convergence study of the post-instability, limit cycle response of the panel. This configuration (geometry, material, freestream conditions) is selected for this study as it has been thoroughly examined in past works [23, 28, 29]. While this configuration does not represent an actual structure intended for use on a hypersonic vehicle, it provides the means to study a representative coupled response over a relatively short time record [28].

Table 27.2 Material properties of Al-7075 at 300 K

Density	2768 kg/m ³
Poisson's ratio	0.325
Modulus of elasticity	71.345 GPa
Specific heat capacity	850.99 J/kg K
Thermal conductivity	132.05 W/m K
Thermal expansion coefficient	22.184 μm/m K

Table 27.3 Numerical parameters of the aerothermoelastic solution

Structural mode shapes	25
Aeroelastic time step	12.5 μs
Aerothermal time step	125 μs

**Fig. 27.4** Transition region as a function of time

27.3 Results and Analysis

A preliminary analysis was performed to demonstrate the importance of accounting for time-varying, fluid stability in aerothermoelastic response prediction. Results are presented for panel responses obtained assuming a constant transition length ($\Delta x_t = 0.2$ m) and an initial transition onset location of $x_t = 0.1$ m. The onset location either remains constant or varies in time as a function of the average wall temperature, according to Eq. (27.16). The relationship in Eq. (27.16) linearly interpolates between $x_t = 0.1$ m, $T_w = 300$ K and $x_t = 0.7$ m, $T_w = 495$ K, where the later conditions are specified to ensure the last 0.1 m of the panel is subject to fully turbulent loading and to remain within the temperature range for the material property data set. Here, Eq. (27.16) is an ad hoc expression meant to approximate the stabilizing effect of elevated temperature on second mode disturbances [6] as the transition onset moves downstream with increasing wall temperature.

$$x_t(t) = 0.1 \text{ m} + (0.7 \text{ m} - 0.1 \text{ m}) \frac{T_w(t) - 300 \text{ K}}{495 \text{ K} - 300 \text{ K}} \quad (27.16)$$

The transition region definitions for the constant and time-varying cases are provided in Fig. 27.4 in terms of the locations corresponding to the onset and end of transition. At the start of the simulation ($t = 0$ s), both cases have the same transition region ($x_t = 0.1$ m, $x_{te} = 0.3$ m). However, as the panel temperature rises, as a result of the applied heat flux, the time-varying transition region moves rearward along the panel, maintaining a transition length of $\Delta x_t = 0.2$ m.

The impact of the time-varying transition region on the panel response is depicted in Fig. 27.5 in terms of the maximum temperature (Fig. 27.5a) throughout the panel and the three quarter chord displacement envelope (Fig. 27.5b). The results in Fig. 27.5 indicate that as the transition region moves rearward along the panel, the peak temperature decreases and the time to flutter increases, as compared to the constant transition region response. This is a product of the reduction in the thermal load, due to the increased region of the panel subject to laminar heating.

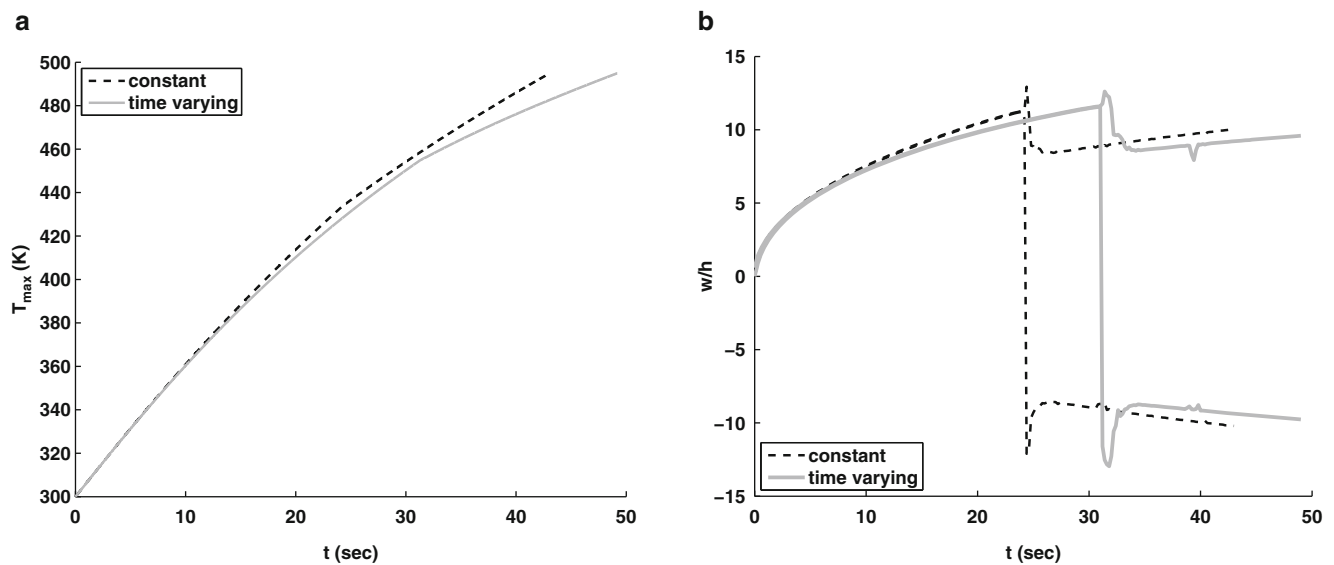


Fig. 27.5 Constant vs. time varying transition location. (a) Maximum temperature. (b) 3/4 chord displacement

The response of the panel subject to both constant and time-varying transitional loads is provided in Fig. 27.6, in terms of the average through-thickness temperature rise (Fig. 27.6a), chordwise thermal gradient (Fig. 27.6b), normalized displacement (Fig. 27.6c), and slope (Fig. 27.6d). Note that, the temperature rise in Fig. 27.6a is relative to the initial panel temperature of 300 K and the displacement in Fig. 27.6c is normalized by the panel thickness h . Comparison of the temperature profiles in Fig. 27.6a, indicates that the time-varying transition region reduces the peak temperature and shifts its spatial location further downstream in time, as compared with the constant transition definition. This reduction and shift in peak temperature greatly reduces the thermal gradient across the panel, as highlighted in Fig. 27.6b. The displacement and slope profiles in Fig. 27.6c, d illustrate that the prescribed transition region only affects the magnitude of the peak deformation. This is expected as the panel deformation is driven by the thermal loading which, as Fig. 27.6a, b highlight, is dependent on the transition region. The asymmetry of the panel is an aeroelastic effect, resulting from the interaction between the fluid pressure and the thermally induced deformation. As the profiles in Fig. 27.6c, d are similar for either transition definition, this implies that the location of the peak fluctuating pressure load does not significantly impact the structural response.

27.4 Conclusions and Future Work

This study examines the effect of time varying boundary layer transition location during aerothermoelastic analysis of a representative hypersonic vehicle panel. The results indicate that rearward movement of the transition front (i.e., relaminarization of the boundary layer) significantly reduces the thermal loading and peak deformation, potentially extending the life of the structure. These results help to quantify the degree of coupling fidelity required to accurately predict the response of a structure subject to hypersonic aerodynamic loading.

Acknowledgements This research was conducted with Government support by the DoD through a National Defense Science and Engineering Graduate Fellowship (32 CFR 168a), the AFRL-University Collaborative Center in Structural Sciences (AFRL/RQ Cooperative Agreement FA8650-13-2-2347) with Dr. Ravi Penmetsa as program manager, and through an allocation of computing time from the Ohio Super Computer Center.

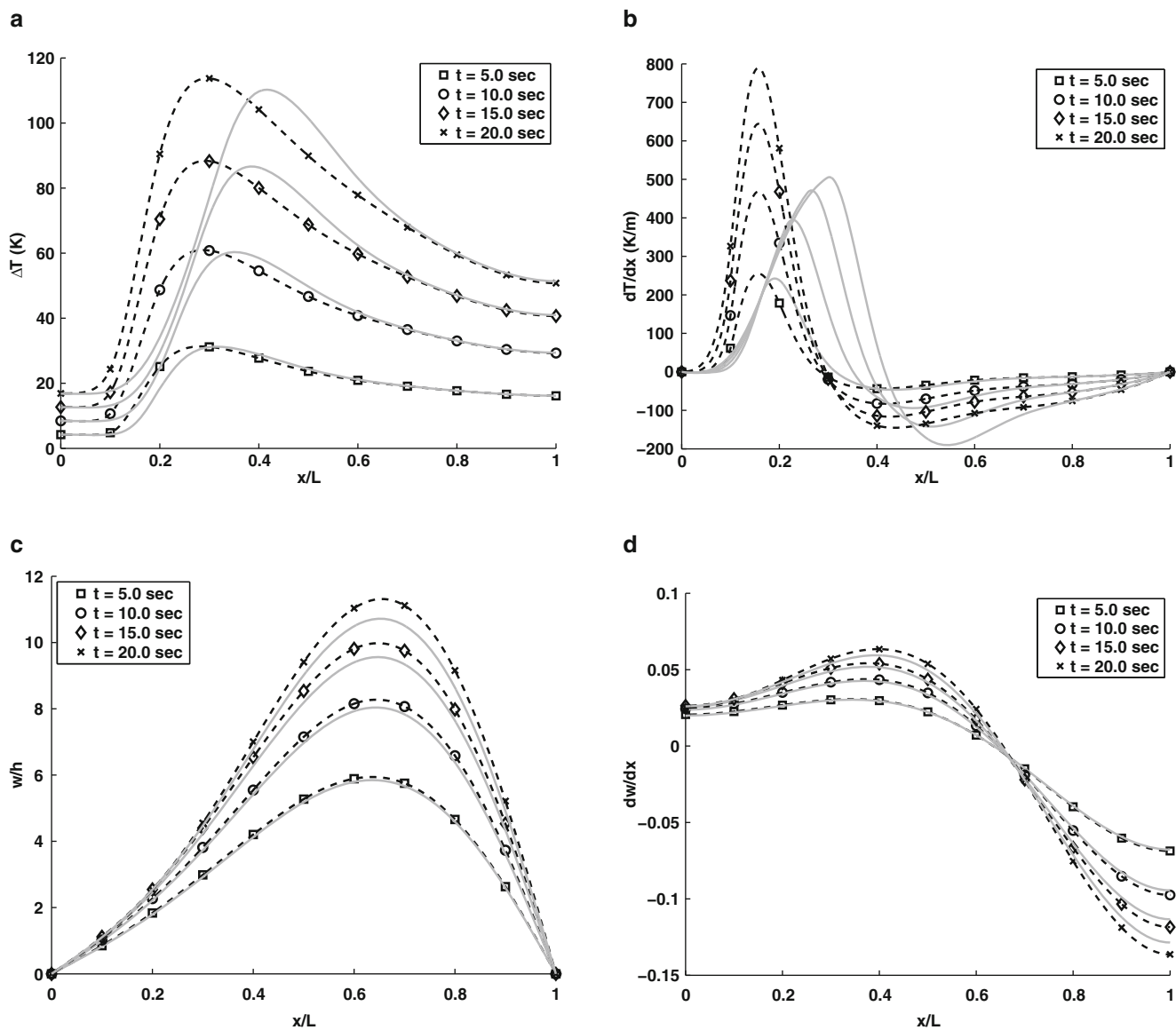


Fig. 27.6 Variation in panel response due to constant (*dashed lines*) and time varying (*solid lines*) transition onset. (a) Average through-thickness temperature rise. (b) Chordwise thermal gradient. (c) Displacement. (d) Slope

References

1. Kontinos, D., Palmer, G.: Numerical simulation of metallic thermal protection system panel bowing. *J. Spacecr. Rocket* **36**(6), 842–849 (1999)
2. Zuchowski, B.: Predictive capability for hypersonic structural response and life prediction, phase I - identification of knowledge gaps. Technical Report AFRL-RB-WP-TR-2010-3069, August 2010
3. Tzong, G., Jacobs, R., Liguore, S.: Predictive capability for hypersonic structural response and life prediction: phase I - identification of knowledge gaps. Technical Report AFRL-RB-WP-TR-2010-3068, September 2010
4. Zuchowski, B.: Predictive capability for hypersonic structural response and life prediction: phase II - detailed design of hypersonic cruise vehicle hot-structure. Technical Report AFRL-RQ-WP-TR-2012-0280, May 2012
5. Quiroz, R., Embler, J., Jacobs, R., Tzong, G., Liguore, S.: Predictive capability for hypersonic structural response and life prediction: phase II - detailed design of hypersonic cruise vehicle hot-structure. Technical Report AFRL-RQ-WP-TR-2012-0265, February 2012
6. Mack, L.M.: The stability of the compressible laminar boundary layer according to a direct numerical solution, pp. 329–362. Technical Editing and Reproduction Ltd., Harford House, 7-9 Charlotte St. London W.1., 97th edn., May 1965, AGARD-CP-97
7. Schneider, S.: Effects of roughness on hypersonic boundary layer transition. *J. Spacecr. Rocket* **45**(2), 193–209 (2008)
8. Fedorov, A., Khokhlov, A.: Receptivity of hypersonic boundary layer to wall disturbances. *Theor. Comput. Fluid Dyn.* **15**, 231–254 (2002)
9. Wang, X., Zhong, X.: Receptivity of a hypersonic flat-plate boundary layer to three-dimensional surface roughness. *J. Spacecr. Rocket* **45**(6), 1165–1175 (2008)

10. Berry, S., Horvath, T.: Discrete-roughness transition for hypersonic flight vehicles. *J. Spacecr. Rocket* **45**(2), 216–227 (2008)
11. Wang, X., Zhong, X.: Effect of wall perturbations on the receptivity of a hypersonic boundary layer. *Phys. Fluids* **21**(4), 19 (2009). Paper 044101. doi:10.1063/1.3103880.
12. Fujii, K.: Experiment of the two-dimensional roughness effect on hypersonic boundary-layer transition. *J. Spacecr. Rocket* **43**(4), 731–738 (2006)
13. Marxen, O., Iaccarino, G., Shaqfeh, E.: Disturbance evolution in a Mach 4.8 boundary layer with two-dimensional roughness-induced separation and shock. *J. Fluid Mech.* **648**, 435–469 (2010)
14. Bountin, D., Chimitov, T., Maslov, A.: Stabilization of a hypersonic boundary layer using a wavy surface. *AIAA J.* **51**(5), 1203–1210 (2013)
15. Duan, L., Wang, X., Zhong, X.: Stabilization of a Mach 5.92 boundary layer by two-dimensional finite-height roughness. *AIAA J.* **51**(1) (2013). doi:10.2514/1.J051643
16. Fong, K., Wang, X., Zhong, X.: Numerical simulation of roughness effect on the stability of a hypersonic boundary layer. *Comput. Fluids* **96**, 350–367 (2014)
17. Fong, K., Wang, X., Zhong, X.: Parametric study on stabilization of hypersonic boundary-layer waves using 2-D surface roughness. AIAA Paper 2015-0837, January 2015, 53rd AIAA Aerospace Sciences Meeting
18. Glass, C.E., Hunt, L.R.: Aerothermal tests of spherical dome protuberances on a flat plate at a Mach number of 6.5. NASA TP-2631 (1986)
19. Glass, C., Hunt, L.: Aerothermal tests of quilted dome models on a flat plate at a Mach number of 6.5, NASA TP-2804 (1988)
20. Berry, S., Horvath, T., Hollis, B., Thompson, R., Hamilton II, H.: X-33 hypersonic boundary-layer transition. *J. Spacecr. Rocket* **38**(5), 646–656 (2001)
21. Riley, Z., McNamara, J., Johnson, H.: Assessing hypersonic boundary layer stability in the presence of structural deformation. *AIAA J.* **52**(11), 2547–2558 (2014). doi: 10.2514/1.J052941
22. Lamorte, N., Friedmann, P.P.: hypersonic aeroelastic and aerothermoelastic studies using computational fluid dynamics. *AIAA J.* **52**(9), 2062–2078 (2014)
23. Riley, Z., Deshmukh, R., Miller, B.A., McNamara, J.: Characterization of structural response to hypersonic boundary layer transition. AIAA Paper 2015-0688, January 2015, 56th AIAA/ASCE/AHS/ASC Structures, Structural Dynamics and Materials Conference
24. Culler, A.J., McNamara, J.J.: Studies on fluid-thermal-structural coupling for aerothermoelasticity in hypersonic flow. *AIAA J.* **48**(8), 1721–1738 (2010)
25. Lighthill, M.: Oscillating airfoils at high Mach numbers. *J. Aeronaut. Sci.* **20**(6), 402–406 (1953)
26. Ashley, H., Zartarian, G.: Piston theory - a new aerodynamic tool for the aeroelastician. *J. Aeronaut. Sci.* **23**(12), 1109–1118 (1956)
27. Eckert, E.R.G.: Engineering relations for heat transfer and friction in high-velocity laminar and turbulent boundary-layer flow over surfaces with constant pressure and temperature. *Trans. ASME* **78**(6), 1273–1283 (1956)
28. Miller, B.A., McNamara, J.J., Culler, A.J., Spottswood, S.M.: The impact of flow induced loads on snap-through behavior of acoustically excited, thermally buckled panels. *J. Sound Vib.* **330**(23), 5736–5752 (2011)
29. Miller, B., McNamara, J.: Efficient time-marching of fluid-thermal-structural interactions. AIAA Paper 2014-0337, January 2014, 55th AIAA/ASME/ASCE/AHS/ASC Structures, Structural Dynamics and Materials Conference
30. Miller, B.A., McNamara, J.J.: Time-marching considerations for response prediction of structures in hypersonic flows. *AIAA J.* **53**(10), 3028–3038 (2015). doi:10.2514/1.J053872
31. Dhawan, S., Narasimha, R.: Some properties of boundary layer flow during the transition from laminar to turbulent motion. *J. Fluid Mech.* **3**, 418–436 (1958)
32. Emmons, H.W.: The laminar-turbulent transition in a boundary layer-Part I. (*Inst. Aeronaut. Sci.*) **18**, 490–498 (1951)
33. Emmons, H.W., Bryson, A.: The laminar-turbulent transition in a boundary layer-Part II. In: *Proceedings of the First U.S. National Congress of Theoretical and Applied Mechanics*, pp. 859–868 (1952)
34. Narasimha, R.: The laminar-turbulent transition zone in the boundary layer. *Prog. Aerosp. Sci.* **22**, 29–80 (1985)
35. Wadhams, T., Mundy, E., MacLean, M., Holden, M.: Ground test studies of the HIFiRE-1 transition experiment part 1: experimental results. *J. Spacecr. Rocket* **45**(6), 1134–1148 (2008)
36. Deshmukh, R., Culler, A., Miller, B., McNamara, J.: Response of skin panels to combined self- and boundary layer- induced fluctuating pressure. *J. Fluids Struct.* **58**, 216–235 (2015)
37. Laganelli, A., Howe, J.: Prediction of pressure fluctuations associated with maneuvering re-entry weapons. AFFDL-TR-77-59, July 1977
38. Laganelli, A., Wolfe, H.: Prediction of fluctuating pressure in attached and separated turbulent boundary-layer flow. *J. Aircr.* **30**(6), 962–970 (1993)
39. Blevins, R.D., Bofilios, D., Holehouse, I., Hwa, V.W., Tratt, M.D., Laganelli, A.L., Pozefsky, P., Pierucci, M.: Thermo-Vibro-Acoustic Loads and Fatigue of Hypersonic Flight Vehicle Structure - Phase II Report, Rohr Industries, Inc., RHR 89-202, November 1989
40. Bull, M.K.: Wall-pressure fluctuations beneath turbulent boundary layers: some reflections on forty years of research. *J. Sound Vib.* **190**(3), 299–315 (1996)
41. Beresh, S.J., Henfling, J.F., Spillers, R.W., Pruett, B.O.: Fluctuating wall pressures measured beneath a supersonic turbulent boundary layer. *Phys. Fluids* **23** (2011). Paper 075110. doi:10.1063/1.3609271